Performance of ITO-free inverted organic bulk heterojunction photodetectors: Comparison with standard device architecture

B. Arredondo [a,*], C. de Dios [b], R. Vergaz [b], A.R. Criado [b], B. Romero [a], B. Zimmermann [c], U. Würfel [c,d]

[a] Dpt. Tecnología Electrónica, Universidad Rey Juan Carlos, C/Tulipán s/n, 28933 Móstoles, Madrid, Spain
[b] Dpt. Tecnología Electrónica, Universidad Carlos III de Madrid, Avda. de la Universidad 30, 28911 Leganés, Madrid, Spain
[c] Fraunhofer Institute for Solar Energy Systems ISE, Heidenhofstr. 2, 79110 Freiburg, Germany
[d] Freiburg Materials Research Center FMF, Stefan-Meier-Str. 21, 79104 Freiburg, Germany

A B S T R A C T

We report on the fabrication of Indium Tin Oxide (ITO)-free inverted organic bulk heterojunction (BHJ) photodetectors of poly(3-hexylthiophene) (P3HT): 1-(3-methoxycarbonyl)-propyl-1-1-phenyl-(6,6) C61 (PCBM). The final inverted device structure is Cr/Al/Cr/P3HT:PCBM/poly-3,4-ethylenedioxythiophene:poly-styrenesulfonate (PEDOT:PSS)/Ag (Zimmermann et al., 2009) [1]. The device is top-absorbing with the light entering through the hole contact grid. We have fabricated standard devices with structure ITO/PEDOT:PSS/P3HT:PCBM/LiF/Al in order to carry out a comparison study. Inverted photodetectors show slightly higher quantum efficiency and responsivity compared to standard devices. Frequency responses at different bias voltages were measured showing a maximum −3 dB cut-off frequency of 780 kHz and 700 kHz at −3 V for the standard and inverted structures respectively. Parameters extracted from the fit of a circuital model to the impedance spectroscopy measurements were used to estimate the photodiode cut-off frequency as function of bias.

1. Introduction

Solution-processable organic solar cells (OSCs) and organic photodetectors (OPDs) based on blends of conjugated polymers (electron donor), and fullerene derivatives (electron acceptor) forming an interpenetrating nanoscale network appear as a promising alternative to inorganic devices due to their potential low cost, light weight and mechanical flexibility. Most studied organic bulk heterojunction devices, typically using the blend P3HT:PCBM as active layer, are bottom absorbing devices with the light entering through the transparent anode, typically ITO. Despite the general use of ITO as transparent electrode, this oxide has inherent disadvantages such as poor transparency in the blue range, high temperature processing, poor sheet resistance which turns out into high device series resistance, and most important, the scarcity of indium increases costs dramatically. Moreover, it has been demonstrated that the system ITO/PEDOT:PSS is unstable with ITO releasing O_2 and In, thus contaminating the organic layer and degrading the device performance [2,3]. Furthermore, ITO is known to be brittle therefore bending can be regarded as highly problematic which makes it a non-ideal candidate for processing on flexible substrates [4,5]. Thus, great efforts are being made to fabricate ITO-free devices following different strategies. Several alternative transparent anodes have been reported: graphene, carbon nanotubes and metal grids [6–13]. In this sense, most studies are focused on fabricating inverted structures that have been developed with the main objective of enhancing device stability by suppressing the ITO/PEDOT interface and thus lowering the manufacturing cost. This inverted architecture usually uses high workfunction metals, stable in air, such as Au and Ag, as anode to collect holes [13–17]. In this context, inverted OSCs have been

* Corresponding author. Tel.: +34 91488 8522; fax: +34 91488 7049.
E-mail address: belen.arredondo@urjc.es (B. Arredondo).

1566-1199/$ - see front matter © 2013 Elsevier B.V. All rights reserved.
http://dx.doi.org/10.1016/j.orgel.2013.06.018

reported with high stability and efficiencies compared to standard ones [1,12,14,17–21]. However, although OSCs and OPDs are similar devices, they have to fulfil different requirements, and only few inverted organic photodetectors have been demonstrated so far [15,16,22]. In contrast to OSC, the spectral region of interest for OPDs is often quite narrow, and the important parameters for detection applications are the responsivity, detectivity and bandwidth. High speed OPDs are required when employed in a wide range of areas such as military, civil and astronomy applications [23–26]. In particular, OPDs for use in wearable applications, optical sensor as well as data transmission systems have received considerable attention [27–29]. The state-of-the-art organic photodetector bandwidth reached 430 MHz for OPDs based on a small molecule [23,30] and 1 MHz for BHJ photodetectors [24].

On the other hand, impedance spectroscopy is often employed to study carrier dynamics in organic devices in dark and under illumination conditions [31,32]. Impedance measurements are fitted with small signal equivalent electric circuits to obtain mobility and carrier characteristic times which in turn can be related to the device bandwidth [33].

In this work we report on a comparative study of standard and inverted ITO-free organic BHJ photodetectors based on the polymer–fullerene blend P3HT:PCBM. OPDs have been characterized in terms of current–voltage characteristic (I–V) in dark and under green LED illumination, external quantum efficiency (EQE) and optoelectronic small signal frequency response (bandwidth) under green LED illumination. OPD responsivities are calculated from the EQE measurements and noise equivalent power (NEP) and specific detectivity (D^*) are calculated from the dark current measured at -1 V. We find that inverted devices show higher responsivity while standard photodetectors present smaller NEP and higher D^* due to a minor dark current density. Cutoff frequencies at -3 dBs have been measured for standard and inverted devices and compared to the ones estimated theoretically from the fit of an equivalent circuit to the impedance measurements at different reverse bias voltages showing good agreement between theory and experiment.

2. Experimental details

2.1. Standard OPD fabrication

Commercial ITO (thickness = 100 nm) coated glass substrates (Präzisions Glas & Optik GmbH, 25 mm × 25 mm) were first manually washed in aqueous detergent, and then sequentially sonicated for 10 min twice in acetone, isopropanol, and once in de-ionised water. They were subsequently blow dried with nitrogen and treated with UV ozone for 20 min afterwards.

The hole transport layer was spin coated from a filtered (0.45 μm PVDF filter) PEDOT:PSS suspension (Clevios Al 4083) at 3000 r.p.m. for 60 s and dried on a hot plate at 130 °C for 10 min. The active layer blend of P3HT (Rieke Metals Inc.):PCBM (Solenne BV), with ratio 1:0.75, in ortho-dichlorobenzene at 3% wt was spin coated at 800 r.p.m. yielding to a thicknesses of ca. 220 nm. Blends were annealed at 150 °C on a hot plate during 15 min. Finally a thin layer of LiF (0.3 nm) and a layer of Al (100 nm) were thermally evaporated on top of the device with a vacuum pressure lower than 10^{-5} mbar.

2.2. Inverted OPD fabrication

Standard glass was used as substrate. The cathode Cr(5 nm)/Al(100 nm)/Cr(5 nm) was deposited by evaporation through a shadow mask. The Cr layers were electron-beam evaporated and the Al layer was thermally evaporated at a pressure lower than 10^{-5} mbar. Before the photoactive layer was deposited, substrates were solvent pretreated with ethanol. The same photoactive blend of P3HT:PCBM solution used for standard devices was spin coated at 800 r.p.m. during 60 s. PEDOT:PSS (Clevios F010) supplied by H.C. Starck was spin coated at 3000 r.p.m. for 60 s. Substrates were annealed at 120 °C during 10 min. Finally a metal Ag (100 nm) grid was thermally evaporated on top of the device at a pressure of 5×10^{-6} mbar. The Ag grid enables the light entering the device.

All devices were encapsulated with a glass tap and an UV-curing adhesive. Except for PEDOT:PSS coating, the whole fabrication process was carried out in a glove-box with N_2 atmosphere. Device active area is 9 mm^2. In this work we compared two samples, one of each type, inverted and standard. Each sample contains six diodes.

This fabrication procedure was first employed by [1,34] to successfully demonstrate organic inverted solar cells.

Fig. 1 shows the device structure for both configurations.

2.3. Electro-optical characterization

EQE was measured with a lock-in amplifier (Stanford Research Systems SRS 830), a 100 W halogen tungsten lamp, a UV808 Newport UV-enhanced silicon detector and a Thorlabs mechanical chopper. I–V characteristics

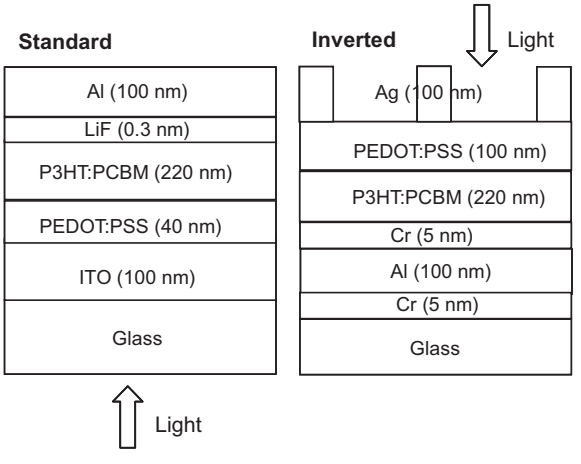

Fig. 1. Schematic illustration of standard and inverted structures.

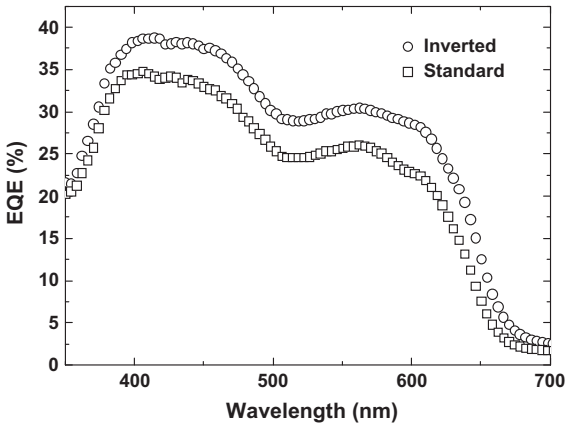

Fig. 2. External quantum efficiency of standard and inverted photodectectors at 0 V.

were carried out with a semiconductor parameter analyzer Agilent 4155C and a source generator Agilent 41501B.

The OPD frequency response was evaluated using the same green LED and modulating the optical emission using a transconductance amplifier that varied the current flow through the LED. The resulting modulated light illuminated the OPD. The detector under study was reverse biased and connected to an equivalent 50 Ω load. Its response has been characterized considering two separate experimental set-ups. The first one, aimed for frequencies below 100 kHz, is based on a high sensitive lock-in amplifier (Stanford Research Systems SRS 830). The second scheme, suitable for frequencies above 60 kHz, relies on an electronic spectrum analyzer (ESA Agilent EXA N910A).

Impedance measurements were carried out with a Solartron 1260 impedance analyzer. The diode was connected to the analyzer that fed the input signal, biasing the diode at different DC levels and superimposing an alternating signal of sweeping frequency with amplitude 100 mV.

I–V curves, OPD frequency response and impedance measurements were all performed illuminating the device with a green LED Vishay TLLG5400 (λ = 530 nm) since absorbance of P3HT:PCBM films presents a maximum at 510 nm [35,36].

Electro-optical measurements in diodes belonging to the same sample were easily reproducible showing low dispersion data.

3. Results and discussion

The EQE measurements in Fig. 2 for both standard and inverted OPDs show similar spectral response with a maximum at 414 nm. The EQE of inverted devices is higher than that of standard ones, with maximum values of 39% and 34% respectively. The mean standard deviation associated to the EQE measurements is less than 5% and 4% for the inverted and standard devices respectively. This deviation is less than the difference between the maximum EQE values of both samples.

Fig. 3 shows the current density versus voltage (*J–V*) curves of the standard and inverted OPDs in dark and under illumination of a green LED. The photocurrent density under reverse bias voltage maintains in a quasi constant range from 3.8 mA/cm^2 at −1 V up to 4 mA/cm^2 at −3 V for both device configurations. The dark current at −1 V was 3.6×10^{-4} mA/cm^2 and 3.8×10^{-3} mA/cm^2 for the standard and inverted photodetectors respectively. This increase of dark current for inverted devices may be attributed to the appearance of leakage currents at the edges of the PEDOT:PSS/Ag grid interface. It is worth mentioning that the fabrication process for both devices was not optimized to obtain low dark currents. At forward bias voltages, dark and illumination currents overlap. Dark *J–V* curves for both devices present an asymmetric behavior with good rectification ratios at ± 1 V of 4.2×10^4 and 2.4×10^4 for standard and inverted OPDs respectively. This asymmetric behavior in reverse and forward bias regions suggests an effective collection of photoinduced charge carriers even at low reverse bias [15].

The responsivity (*R*, A/W) of a photodetector is a figure of merit giving the device transfer characteristic, i.e. the photocurrent per unit incident optical power. *R* can be estimated in terms of the wavelength of the incident light and quantum efficiency as,

$$R = \frac{\eta e \lambda}{hc} \tag{1}$$

where *e* is the electron charge, λ is the wavelength, *h* is the Plank constant, *c* is the light velocity and η is the quantum efficiency. As was expected from the EQE measurements, the responsivity is found to be slightly higher for inverted devices, with values of 0.11 A/W and 0.13 A/W at 530 nm for the standard and inverted devices respectively. The noise equivalent power (*NEP*, in W/Hz$^{1/2}$) defined as the incident optical power at a particular wavelength required to produce a photodetector current equal to the rms noise current [37] is given by,

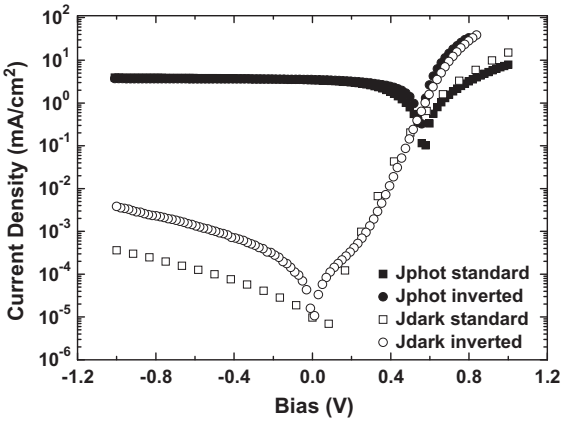

Fig. 3. Photogenerated current density under greed LED illumination (filled symbols) and current density in dark (hollowed symbols) for standard and inverted OPDs.

$$NEP = \frac{\sqrt{\langle I_N^2 \rangle / B}}{R} \tag{2}$$

where I_N is the noise current, B the bandwidth (=1 Hz) and R is the responsivity. Assuming that the shot noise current associated to the dark current is dominant over the thermal noise, *NEP* can be expressed as,

$$NEP = \frac{\sqrt{\langle I_N^2 \rangle}}{R} = \frac{\sqrt{2eI_D}}{R} \tag{3}$$

where I_D is the photodetector dark current. We obtain a dark current *NEP* of 9.5×10^{-13} W/Hz$^{1/2}$ and 2.6×10^{-12} W/Hz$^{1/2}$ for standard photodetectors and inverted devices respectively. We can conclude from these values that the better responsivity of inverted devices cannot make up for its high dark current, resulting in worsening of the *NEP*. The specific detectivity (D^*, Jones) is an area independent figure of merit in detectors indicating the ability to detect lower levels of incident power. D^* can be written as,

$$D^* = \frac{\sqrt{A}}{NEP} \tag{4}$$

where A is device area ($A = 9$ mm^2). We calculate a D^* of 3.15×10^{11} Jones for standard devices and 1.2×10^{11} Jones for inverted ones. Table 1 summarizes the photodiodes most relevant parameters.

Fig. 4 shows the normalized modulation response of the OPD at −1 V and −3 V. Measurements carried out with the lock-in amplifier (up to 100 kHz) are shown along with the characterization performed with the high frequency ESA (from 60 kHz upwards). It is worth saying that the Electrical Spectrum measurements have been averaged over 10 traces for each point, while the Lock-In measurements have been integrated over 1 s. This should lead to a minimum uncertainty given by random variations of the measurements. The photodetector bandwidth is similar for both configurations and increases with reverse bias reaching up to 780 kHz for standard devices and 700 kHz for inverted ones at −3 V. These values are higher than that measured for similar organic standard BHJ photodetectors [16,29,38] and very close to the state-of-the-art [24]. In fact, comparing our devices with similar ITO-free inverted OPDs, devices presented in this work show almost double bandwidth than those reported by other authors [22]. It is worth noticing that this OPD speed is high enough for many communications and instrumentation applications. Further increasing bias does not significantly improve the −3 dB cutoff frequency. Standard devices present a bandwidth approximately 10% higher than that of inverted devices. On the other hand, R follows the opposite tendency, i.e., it is about 15% higher for inverted devices.

Impedance spectroscopy measurements give a straightforward estimation of the electrical parameters modeling

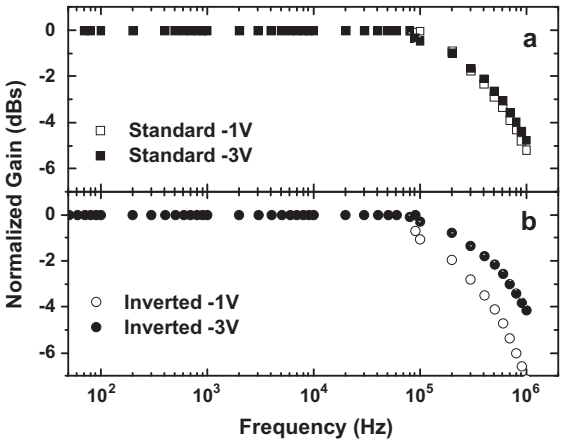

Fig. 4. Optoelectronic small signal frequency response of the standard (a) and inverted (b) OPDs biased at −1 V and −3 V under modulated green-LED illumination. Frequency response was characterized with a 100-kHz lock-in amplifier setup and an electronic spectrum analyzer from 60 kHz upwards.

the device through simple equivalent circuits. Fig. 5 depicts the electrical impedance measured under green LED illumination conditions in the 10 Hz–10 MHz frequency range at different bias. The spectra for standard and inverted devices resemble the classical behavior of a slightly depressed semicircle. Several equivalent electrical circuits have been used to model the experimental impedance [31,32] though the simplest one is displayed in the inset of Fig. 5a. It consists of a resistance R_s in series with a parallel set of a capacitor (C) and a parallel resistance R_p. This resistance accounts for the parallel of the diode dynamical resistance and shunt resistance and thus it includes both material characteristics such as carrier mobility and leakage currents due to fabrication defects and device geometry. R_S is a series resistance modeling metallic contacts, wires, the sheet resistance of the PEDOT:PSS hole transport layer, etc. The capacitor C models the dielectric effects of the blend. The equivalent impedance of the circuit shown in the inset of Fig. 5 is,

$$Z_{eq} = R_S + \frac{R_P \cdot Z_C}{R_P + Z_C} \tag{5}$$

Impedance fits were carried out taking into account three circuital parameters: C, R_P and R_S. Solid lines in Fig. 5 show the fits of Eq. (5) to the experimental data, with good agreement especially at high bias. Table 2 displays the parameters extracted from the fit at different bias with an error less than 5%. R_S is found to be around 40 Ω and C ranges from 1.3 nF to 1.9 nF for both devices. Parameters in Table 2 have been related to the −3 dB cutoff frequency using the method proposed in [33]. Under incident modulated light, the dynamic optoelectronic

Table 1
Summary of OPD parameters at bias −1 V.

	J_{dark} (mA/cm^2)	R (A/W)@530 nm	*NEP* (W/Hz$^{1/2}$)	D^* (Jones)
Standard	3.6×10^{-4}	1.1×10^{-1}	9.5×10^{-13}	3.15×10^{11}
Inverted	3.8×10^{-3}	1.3×10^{-1}	2.6×10^{-12}	1.2×10^{11}

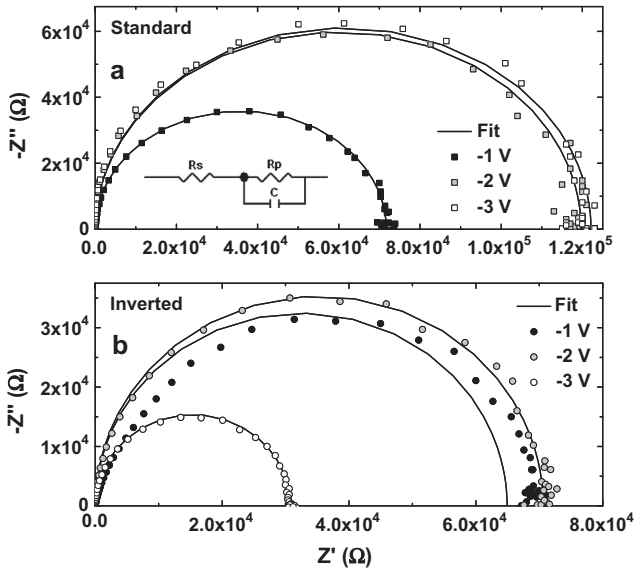

Fig. 5. Impedance spectra measured under illumination conditions of green LED at different bias (symbols) for standard (a) and inverted (b) photodetector. Inset shows the equivalent circuit used to model the impedance. Solid lines show the fit to the circuit in the inset.

Table 2
Circuital parameters obtained from the fit of Fig. 5.

	−1 V	−2 V	−3 V
C_{std} (nF)	1.6	1.4	1.4
C_{inv} (nF)	1.9	1.5	1.5
R_{Pstd} (kΩ)	71.6	119.6	122.1
R_{Pinv} (kΩ)	64.9	70.6	30.7

response of the OPD can be modeled with the circuit shown in the inset of Fig. 6. Since bandwidth and impedance measurements are performed in the small signal domain under the same illumination conditions we can use

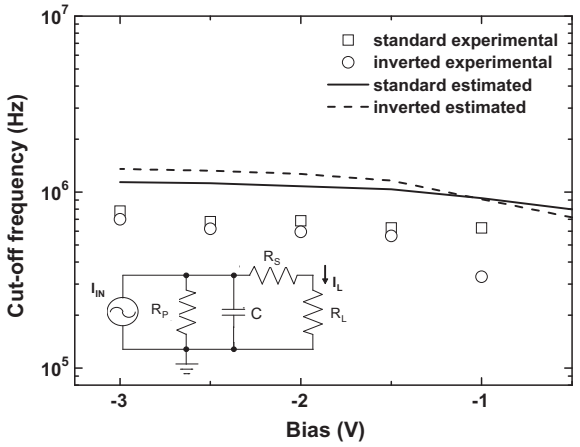

Fig. 6. Experimental (hollowed symbols) and calculated (line) cutoff frequencies versus bias for standard and inverted photodetectors. Inset shows the AC equivalent circuit for the OPD in the cutoff frequency measurement.

the parameters in Table 2 to calculate the −3 dB cutoff frequencies from the transfer function of the small signal equivalent circuit of Fig. 6 as,

$$\frac{I_L}{I_{IN}} = \frac{\frac{R_P \cdot Z_C}{R_P + Z_C}}{\left(\frac{R_P \cdot Z_C}{R_P + Z_C}\right) + (R_L')} = \frac{R_P}{(R_P + R_L')\left(1 + j\omega \frac{CR_P R_L'}{R_P + R_L'}\right)} \tag{6}$$

with $R_L' = R_L + R_S$ and $R_L = 50\ \Omega$ the load resistance. Eq. (6) shows a pole (−3 dB cutoff frequency) at

$$f_C = \frac{1}{2\pi \cdot C\left(\frac{R_P \cdot R_L'}{R_P + R_L'}\right)} \approx \frac{1}{2\pi \cdot CR_L'} (R_P >> R_L') \tag{7}$$

Fig. 6 shows good agreement between experimental and calculated cutoff frequencies for inverted and standard devices at different bias. Cutoff frequency is overestimated when it is calculated with the above mentioned method. This can be partially due to the frequency response of the additional electronic circuitry used to measure the photodetector bandwidth. At −1 V the obtained theoretical (experimental) f_c is 925 kHz (625 kHz) and 910 kHz (330 kHz) for the standard and inverted devices respectively, while at −3 V the f_c is 1.1 MHz (780 kHz) and 1.3 MHz (700 kHz) for the standard and inverted devices respectively. It can be concluded that when the impedance measurements do not fit well with a simple capacitor model, as in the case of the inverted cell at −1 V, the estimated f_c is far from the experimental value. In this case, interface or surface effects may take place, and more complex models including non-ideal circuital components such as constant phase elements (CPE) should be considered [33].

4. Conclusions

In conclusion we have demonstrated ITO-free top-absorbing inverted photodetectors showing similar perfor-

mance to standard devices in terms of responsivity and bandwidth. Photodetectors show good current rectification ratios >10^4 at ± 1 V and an almost equally good −3 dBs cut-off frequency of 780 kHz and 700 kHz at −3 V for standard and inverted devices respectively. These values are a state-of-the-art bandwidth for inverted devices and high enough for many organic high speed optical communication systems. Responsivity of inverted devices is 0.13 A/W, slightly higher than that of standard devices, due to higher quantum efficiency. Inverted OPDs show a vaguely higher NEP and lower specific detectivity as a result of a higher dark current density. This may be attributed to higher leakage currents at the anode Ag grid interface. ITO-free OPDs drastically reduce the fabrication costs, suggesting that this type of devices can be integrated cost-effectively in a wide variety of applications.

Acknowledgements

Authors would like to acknowledge Dr. J. Cabanillas and G. del Pozo for his help with the EQE measurements. This work has been supported by Comunidad Autónoma de Madrid and Universidad Rey Juan Carlos under project S2009/ESP-1781.

References

[1] B. Zimmermann, U. Würfel, M. Niggemann, Longterm stability of efficient inverted P3HT:PCBM solar cells, Sol. Energy Mater. Sol. Cells 93 (2009) 491–496.
[2] M.P. de Jong, L.J. van I. Jzendoorn, M.J.A. de Voigt, Stability of the interface between indium-tin-oxide and poly(3,4-ethylenedioxythiophene)/poly(styrenesulfonate) in polymer light-emitting diodes, Appl. Phys. Lett. 77 (2000) 2255–2257.
[3] S. Schäfer, X.J. Feng, T. Mayer, A. Petersen, T.A. Wagner, R. Kniprath, D. Lingenfelser, A. Zen, T. Kirchartz, B. Zimmermann, U. Würfel, Influence of the Indium Tin Oxide/organic interface on open-circuit voltage, recombination, and cell degradation in organic small-molecule solar cells, Phys. Rev. B 83 (2011) 165311–165324.
[4] Z. Chen, B. Cotterell, W. Wang, The fracture of brittle thin films on compliant substrates in flexible displays, Eng. Fract. Mech. 69 (2002) 597–603.
[5] K. Alzoubi, M. Hamasha, S. Lu, B. Sammakia, Bending fatigue study of sputtered ITO on flexible substrate, Display Technol., J. 7 (2011) 593–600.
[6] M.W. Rowell, M.A. Topinka, M.D. McGehee, H.-J. Prall, G. Dennler, N.S. Sariciftci, L. Hu, G. Gruner, Organic solar cells with carbon nanotube network electrodes, Appl. Phys. Lett. 88 (2006) 233506–233508.
[7] S. Pang, Y. Hernandez, X. Feng, K. Müllen, Graphene as transparent electrode material for organic electronics, Adv. Mater. 23 (2011) 2779–2795.
[8] H. Park, J.A. Rowehl, K.K. Kim, V. Bulovic, J. Kong, Doped graphene electrodes for organic solar cells, Nanotechnology 21 (2010) 505204.
[9] D.-S. Leem, A. Edwards, M. Faist, J. Nelson, D.C. Bradley, J.C. de Mello, Efficient organic solar cells with solution-processed silver nanowire electrodes, Adv. Mater. 23 (2011) 4371–4375.
[10] T. Ameri, G. Dennler, C. Waldauf, H. Azimi, A. Seemann, K. Forberich, J. Hauch, M. Scharber, K. Hingerl, C.J. Brabec, Fabrication, optical modeling, and color characterization of semitransparent bulk-heterojunction organic solar cells in an inverted structure, Adv. Funct. Mater. 20 (2010) 1592.
[11] F.C. Krebs, All solution roll-to-roll processed polymer solar cells free from indium-tin-oxide and vacuum coating steps, Org. Electron. 10 (2009) 761–768.
[12] B. Zimmermann, H.-F. Schleiermacher, M. Niggemann, U. Würfel, ITO-free flexible inverted organic solar cell modules with high fill factor prepared by slot die coating, Sol. Energy Mater. Sol. Cells 95 (2011) 1587–1589.
[13] P. Kopola, B. Zimmermann, A. Filipovic, H.-F. Schleiermacher, J. Greulich, S. Rousu, J. Hast, R. Myllylä, U. Würfel, Aerosol jet printed grid for ITO-free inverted organic solar cells, Sol. Energy Mater. Sol. Cells 107 (2012) 252–258.
[14] H. Jin, C. Tao, M. Velusamy, M. Aljada, Y. Zhang, M. Hambsch, P.L. Burn, P. Meredith, Efficient, large area ITO-and-PEDOT-free organic solar cell sub-modules, Adv. Mater. 24 (2012) 2572–2577.
[15] X. Liu, H. Wang, T. Yang, W. Zhang, I.-F. Hsieh, S.Z.D. Cheng, X. Gong, Solution-processed near-infrared polymer photodetector with an inverted device structure, Org. Electron. 13 (2012) 2929–2934.
[16] D. Baierl, B. Fabel, P. Gabos, L. Pancheri, P. Lugli, G. Scarpa, Solution-processable inverted organic photodetectors using oxygen plasma treatment, Org. Electron. 11 (2010) 1199–1206.
[17] J. Ajuria, I. Etxebarria, W. Cambarau, U. Muñecas, R. Tena-Zaera, J.C. Jimeno, R. Pacios, Inverted ITO-free organic solar cells based on p and n semiconducting oxides. New designs for integration in tandem cells, top or bottom detecting devices, and photovoltaic windows, Energy Environ. Sci. 4 (2011) 453–458.
[18] C.-H. Hsieh, Y.-J. Cheng, P.-J. Li, C.-H. Chen, M. Dubosc, R.-M. Liang, C.-S. Hsu, Highly efficient and stable inverted polymer solar cells integrated with a cross-linked fullerene material as an interlayer, J. Am. Chem. Soc. 132 (2010) 4887–4893.
[19] T. Yang, W. Cai, D. Qin, E. Wang, L. Lan, X. Gong, J. Peng, Y. Cao, Solution-processed zinc oxide thin film as a buffer layer for polymer solar cells with an inverted device structure, J. Phys. Chem. C 114 (2010) 6849–6853.
[20] Y. Sun, J.H. Seo, C.J. Takacs, J. Seifter, A.J. Heeger, Inverted polymer solar cells integrated with a low-temperature-annealed Sol–Gel-derived ZnO film as an electron transport layer, Adv. Mater. 23 (2011) 1679–1683.
[21] T. Ameri, G. Dennler, C. Waldauf, P. Denk, K. Forberich, M.C. Scharber, C.J. Brabec, K. Hingerl, Realization, characterization, and optical modeling of inverted bulk-heterojunction organic solar cells, J. Appl. Phys. 103 (2008) 084506.
[22] D. Baierl, B. Fabel, P. Lugli, G. Scarpa, Efficient indium-tin-oxide (ITO) free top-absorbing organic photodetector with highly transparent polymer top electrode, Org. Electron. 12 (2011) 1669–1673.
[23] P. Peumans, V. Bulovic, S.R. Forrest, Efficient, high-bandwidth organic multilayer photodetectors, Appl. Phys. Lett. 76 (2000) 3855–3857.
[24] M. Punke, S. Valouch, S.W. Kettliz, N. Christ, C. Gärtner, M. Gerken, U. Lemmer, Dynamic characterization of organic bulk heterojunction photodetectors, Appl. Phys. Lett. 91 (2007) 071118.
[25] F.-C. Chen, S.-C. Chien, G.-L. Cious, Highly sensitive, low-voltage, organic photomultiple photodetectors exhibiting broadband response, Appl. Phys. Lett. 97 (2010) 103301–103303.
[26] L. Zhu, Q. Dai, Z.-F. Hu, X.-Q. Zhang, Y.-S. Wang, High response organic deep ultraviolet photodetector with PEDOT:PSS anode, Opt. Lett. 36 (2011) 1821–1823.
[27] M. Punke, S. Valouch, S.W. Kettlitz, M. Gerken, U. Lemmer, Optical data link employing organic light-emitting diodes and organic photodiodes as optoelectronic components, J. Lightwave Technol. 26 (2008) 816–823.
[28] M. Barbaro, A. Caboni, P. Cosseddu, G. Mattana, A. Bonfiglio, Active devices based on organic semiconductors for wearable applications, IEEE Trans. Inf Technol. Biomed. 14 (2010) 758–766.
[29] L. Salamandra, G. Susanna, S. Penna, F. Brunetti, A. Reale, Time-resolved response of polymer bulk-heterojunction photodetectors, IEEE Photonic Technol. Lett. 23 (2011) 780–782.
[30] P. Peumans, A. Yakimov, S.R. Forrest, Small molecular weight organic thin-film photodetectors and solar cells, J. Appl. Phys. 93 (2003) 3693–3723.
[31] G. Garcia Belmonte, A. Munar, E.M. Barea, J. Bisquert, I. Ugarte, R. Pacios, Charge carrier mobility and life time of organic bulk heterojunctions analyzed by impedance spectroscopy, Org. Electron. 9 (2008) 847–851.
[32] G. Perrier, R. de Bettignies, S. Berson, N. Lemaitre, S. Guillerez, Impedance spectrometry of optimized standard and inverted P3HT-PCBM organic solar cells, Sol. Energy Mater. Sol. Cells 101 (2012) 210–216.
[33] B. Arredondo, C. De Dios, R. Vergaz, G. Del Pozo, B. Romero, High-bandwidth organic photodetector analyzed by impedance spectroscopy, IEEE Photonic Technol. Lett. 24 (2012) 1868–1871.
[34] M. Glatthaar, M. Niggemann, B. Zimmermann, P. Lewer, M. Riede, A. Hinsch, J. Luther, Organic solar cells using inverted layer sequence, Thin Solid Films 491 (2005) 298–300

[35] G. Grancini, D. Polli, D. Fazzi, J. Cabanillas-Gonzalez, G. Cerullo, G. Lanzani, Transient absorption imaging of P3HT:PCBM photovoltaic blend: evidence for interfacial charge transfer state, J. Phys. Chem. Lett. 2 (2011) 1099–1105.
[36] V. Shrotriya, J. Ouyang, R.J. Tseng, G. Li, Y. Yang, Absorption spectra modification in poly(3-hexylthiophene):methanofullerene blend thin films, Chem. Phys. Lett. 411 (2005) 138–143.
[37] J.M. Senior, Optical Fiber Communications. Principles and Practice, second ed., Prentice Hall International Series in Optoelectronics, 1992.
[38] M. Ramuz, L. Bürgi, C. Winnewisser, P. Seitz, High sensitivity organic photodiodes with low dark currents and increased lifetimes, Org. Electron. 9 (2008) 369–376